

High fidelity physiological blood flow in patient-specific arteriovenous fistula for clinical applications

McCullough, J.W.S.¹ and Coveney, P.V.^{1,2}

¹*Centre for Computational Science, Department of Chemistry, University College London, UK*

²*Informatics Institute, University of Amsterdam, Netherlands*

May 17, 2022

Abstract

An arteriovenous fistula, created by artificially connecting segments of a patient's vasculature, is the preferred way to gain access to the bloodstream for kidney dialysis. The increasing power and availability of supercomputing infrastructure means that it is becoming more realistic to use simulations to help identify the best type and location of a fistula for a specific patient. We describe a 3D fistula model that uses the lattice Boltzmann method to simultaneously resolve blood flow in patient-specific arteries and veins. The simulations conducted here, with vasculatures of the whole forearm, have been validated against peroperative clinical data with very good agreement. This demonstrates our ability to provide practical solutions to clinical problems with *in silico* methods and that such approaches provide valuable means with which to plan interventions. This aspect of our work underscores the strategic importance of developing virtual human-scale physiological models for basic and clinical medicine.

Keywords— Blood Flow Modelling, Lattice Boltzmann Method, Arteriovenous Fistula, Surgical Planning, Patient Specific Modelling

1 Introduction

The development of the virtual human to recreate an individual’s specific physiological processes in a digital format is a major goal of computational biomedicine, heralding truly personalised medicine along with ‘healthcasts’ [1, 2, 3, 4, 5, 6, 7]. The increasing capability and power of computational software and hardware has allowed significant steps to be made towards this goal [1, 8]. The development of such a ‘digital doppelganger’ is not a strict progression from low-level (e.g. genomic and DNA studies) to high-level (e.g. organ modelling or epidemiological phenomena) processes but both top-down and bottom-up [9]. The purpose of the present paper is to report a further advance to these efforts, specifically in the field of blood flow modelling. While 3D flow in large arterial structures has been simulated [10, 11], we demonstrate how scalable 3D modelling codes can be used to examine macroscopic blood flow in coupled arteries and veins at human scale. We will discuss how the capillary beds linking the two networks in a virtual human can be captured in an efficient manner and demonstrate how such *in silico* models can be utilised to assist in planning vascular surgery.

The flow of blood around the body is fundamental for the transport and processing of oxygen, nutrients, drugs, and waste products. This is a multiscale process encompassing molecular level chemical exchange, microscopic

cellular motion and macroscopic motion of whole blood. As the development of the virtual human progresses, knowledge at all these levels will be necessary to correctly simulate an individual's physiological processes. At the macroscopic scale, blood may be treated as a continuum fluid that behaves according to the Navier-Stokes equations for fluid flow. Many studies solve these equations for vascular networks through the use of highly simplified 1D representations. The specific properties of an individual's vascular network are used as input for nodal locations within such 1D models [12, 13, 14, 15]. This approach has advantages relating to the relative ease in parameterisation of the model and the computational effort required to reach a solution. In comparison, 3D models permit a far higher fidelity study of the blood flow by means of an exact representation of the domain of interest and do not rely on major assumptions about flow behaviour (e.g. symmetry) that are made by 1D solvers [10, 11, 16]. However, 3D simulations are more demanding to execute. As supercomputers become more powerful, it is more tractable to study 3D flow of large, human-scale, vascular domains [10, 11, 16]. Studies of this nature are better equipped to reveal the subtle phenomena that exist within complex vasculatures. To take advantage of increasing computational performance, a numerical method that demonstrates excellent parallel scaling capability whilst studying complex geometries is essential. In the development of the virtual human, such performance will allow an *in silico* model to generate necessary data and provide this to a patient's healthcare team in a timely fashion. The lattice Boltzmann method (LBM) used in this work is an ideal candidate for meeting these requirements due to its easily parallelised algorithm and often localised approach to solving the complex geometries or

moving boundaries found at multiple scales in blood flow [17, 18, 19].

Irrespective of whether a 1D or 3D model is used to represent the systemic blood vessels, there will remain sections of the vascular network, vital for physiological function, that must be approximated as sub-scale material. A typical instance of this is the flow through the capillary beds that feed the muscles and skin throughout the body. These vessels are too small to be resolved with typical scanning techniques used to obtain geometries of larger vessels. For instance, typical MRI scans used in hospitals can typically only resolve features larger than 1mm [20]. Alternate scanning techniques may achieve improved resolution - computed tomography (CT) 0.5mm and ultrasound 0.15mm - typically at the cost of lower contrast resolution [21]. The flow behaviour within these unresolved vessels becomes incorporated into the boundary conditions of macroscopic flow models. The development of a self-coupled version of the LBM code used in this study, HemeLB, has been used to show how this framework can simulate flow in human-scale arteries and veins [16].

We provide a contextual setting for this work by examining 3D flow through a personalised representation of the major arteries and veins in the human forearm. For patients suffering from kidney failure who require haemodialysis to remove waste products from the bloodstream, an arteriovenous fistula is a common course of action to facilitate treatment [22, 23]. This procedure typically links a vein in the forearm to an arterial branch. Bypassing the tissue increases the blood flow through the vein, in turn in-

creasing the size and strength of the vessel. Once matured, the vein is then used as an access point for blood to be removed for dialysis and returned to the body. The utilisation of *in silico* models prior to treatment permits surgeons to assess different treatment options prior to undertaking invasive procedures [22, 23]. In this work we examine flow through the left forearm vessels illustrated in Figure 1. Firstly we study flow in unmodified vessels to assess baseline parameters prior to treatment. Following this we demonstrate how the model can be used to assess a candidate fistula location and its impact on vessels throughout the arm.

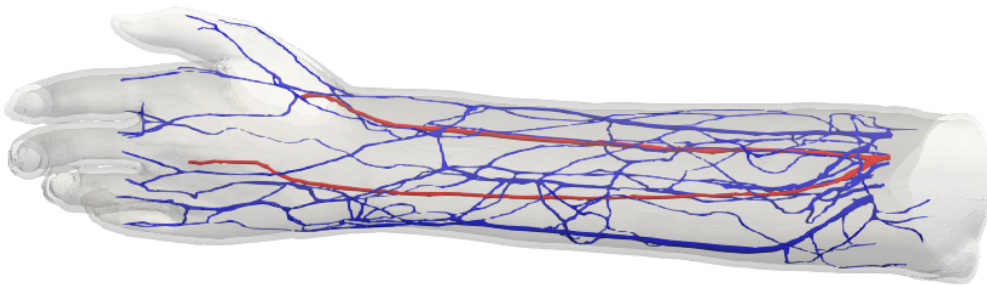


Figure 1: Human scale vessels in the left forearm. Arteries are coloured red and the veins in blue.

Within the literature, there exists a number of *in silico* models for studying arteriovenous fistula creation and its application to surgical planning and evaluation, for example [24, 25, 26, 27, 28, 29]. Of these, cases that capture large-scale vascular domains are typically 1D studies [24, 26, 28] whilst 3D studies [25, 27, 29] typically only focus on the region of the fistula and do not consider the wider arterial and venous networks throughout the arm. In our model we are able to combine these two features by efficiently simulating 3D

resolved flow in detailed networks of large-scale vessels. This is an important step as factors dictating the success of a fistula depend on flow in both the created junction and throughout the remainder of the arm.

In what follows we discuss the formulation of our *in silico* model. We use this to analyse flow in normal arteries and veins within the left forearm and those that have been modified to incorporate an arteriovenous fistula. We compare our results to those reported in clinical studies and demonstrate excellent agreement.

2 Methods

We employ the LBM-based solver HemeLB [30] to simulate macroscopic blood flow in coupled arterial and venous geometries. Further technical information on the LBM can be found in the many textbooks that cover this topic in detail (e.g. [31, 32, 33, 34, 35]). HemeLB is an open-source code that has been optimised for the study of flow in sparse geometries such as those typical of vascular networks. Since its inception [36], HemeLB has been used to study problems including flow validation in cerebral vessels [18], haemodynamic force distributions in retinal vessels [37] and wall shear stress analysis [38, 39, 40] in cerebral arteries, and the transport of magnetic nanoparticles for drug delivery within the circle of Willis [41]. These studies demonstrate how HemeLB, and 3D modelling techniques more generally, are able to accurately capture complex physiological flow phenomena in ways that are not

possible with 1D approaches and can be difficult or impossible to measure and assess directly within a patient. In this work, we implement velocity inlet boundary conditions and pressure outlet conditions utilising the methods described in previous publications using HemeLB [42]. In this work, we assume that solid walls are rigid with fluid-solid interfaces implemented using the technique of Bouzidi et al. [43].

We build on the self-coupled HemeLB presented in our previous work [16], which linked two instances of HemeLB in order to capture the respective flow in arterial and venous geometries. The scheme implemented here was designed to streamline the amount of data transferred between the two instances. In subsequent testing, we have demonstrated the strong scaling of this coupled model up to 30,000 computer cores on the supercomputer SuperMUC-NG (Leibniz Supercomputing Centre, Germany).

2.1 Sub-scale representation of capillary beds

In this work we outline one method designed to represent the capillary beds linking the arterial and venous geometries that cannot be fully resolved for macroscopic simulations. This begins by first mapping the arterial outlets to the venous inlets. The separate collections of these represent individual beds. For any given bed, the sub-scale model needs to be able to accommodate an arbitrary number of arteries and veins being connected. In most regions of the body, there are significantly more veins than arteries of simulatable scale.

This means that most beds will have n arteries and m veins connected where typically $n < m$. Local vascular features, however, may result in alternative configurations. In the current work we identify bed regions and use the sub-scale model to represent the capillaries connecting the arteries and veins located within that region.

Within this model, we use the average velocities from vessels on the opposite geometry to update those on the current set of vessels. The change in velocity here represents the action of the sub-scale capillary network on the flow. Coupling occurs at specified simulation intervals and we alternate the direction of coupling at each instance. As the LBM represents a quasi-incompressible fluid, we use the updated velocities on the arterial geometry to apply a force to the outlets based on the dynamic pressure at that outlet. This represents the volume of fluid within the sub-scale region. This forcing term is applied at the outlet using the approach of Guo et al. [44].

The approach used in this paper is based on one we first described in [16]. In this model we assign a pressure drop between a given vessel and the mean location of its own vessel type. This factor is chosen to represent physiologically expected values seen in capillary beds. For example, the pressure drop between that at the mean arterial outlet location, P_0 , and the individual artery, P_j , can be expressed as

$$\Delta P_j = P_0 - P_j = k_j q_j L_j, \quad (1)$$

where the drop is proportional to the flow rate, q_j , and distance between them, L_i . This can then be represented as a ratio in comparison to the pressure at the arterial vessel. By examining the units of the constant of proportionality, k_j , it can be noted that this factor is itself inversely proportional to the area of the vein, A_j . These quantities then allow a scaling factor for velocity, v_j/v_0 , between the linked vessels to be computed using

$$\frac{v_j}{v_0} = \frac{A_0 \Delta P_j L_1 A_j}{A_j \Delta P_1 L_j A_1} \left(\sum_{k=1}^m \frac{\Delta P_k L_1 A_k}{\Delta P_1 L_k A_1} \right)^{-1}. \quad (2)$$

This relationship can be obtained by ensuring mass conservation between the connecting vessels. When coupling the arteries and veins together, the flow velocity at the mean vessel location is determined from the flow at vessels in the opposite bed. To illustrate this we describe the calculation of velocities used at venous inlets from those at arterial outlets. Firstly we determine the flow at the mean arterial location by scaling the mean velocity at each outlet by the appropriate velocity factor and taking the average of these. The flow at the mean venous location is then determined by conserving mass flow from the mean arterial location, this is done using the total areas of arteries and veins. The velocity at individual veins is then determined by scaling the value at the mean venous location by the relevant scaling factor.

Throughout this work we compared the results of this method to an alternative approach, outlined in the Supplementary Information, based on the resistor-capacitor models used in some existing models of capillary beds or windkessel boundary conditions. We observed no significant difference in the

performance of these methods but believe that the approach outlined above to be a more robust implementation. There may be applications where the alternative is more suitable.

3 Results

We applied the sub-scale method discussed in Section 2.1 to a large model of human blood vessels. This domain consists of the left forearm of the full human Yoon-sun model [45] (Figure 1), which is available as part of the Virtual Population (ViP) library [46, 47]. The segmentation of the full human model domain meant that the finest vessels in this domain had a diameter of approximately 0.4mm. We discretised these geometries to a resolution of $\Delta x = 25 \mu m$, resulting in a total of 64,998,754 lattice sites in the arterial geometry and 166,652,137 in the venous geometry. We conducted simulations with a time step of $\Delta t = 2 \mu s$, resulting in a LBM single relaxation time parameter of $\tau = 0.5384$. These discretisation parameters were selected based on two key considerations. The first, governing Δx , was that the finest vessels were sufficiently well resolved to capture the flow within them. The second was that Δt (and by corollary τ) permitted the LBM method to stably solve flow within the expected physiological values. The values chosen meet our expectations for these criteria. All test cases were run for a total of 2 million time steps. This corresponds to 4 s of physical time being simulated and demonstrates the capacity of our model to efficiently represent multiple cardiac cycles. These were conducted on SuperMUC-NG and each took ap-

proximately 2.5 hours of wall time to run on 1500 nodes (72,000 cores).

To demonstrate our model captures the flow behaviour expected within an arteriovenous fistula we consider four cases. The first is a ‘healthy’ case where we apply a typical flow waveform to the unmodified domains with a single capillary bed region (all venous inlets in the hand region are fed by the two arterial outlets). In the remaining three cases we demonstrate how our model can capture an arteriovenous fistula. A common option for creating a fistula is to connect between the radial artery and cephalic vein [48]. This connection bypasses the capillaries in the hand and serves to increase blood flow in the cephalic vein. In the first of our examples, we attempt to replicate such a fistula solely by modifying the coupling map between the arteries and veins. In the second and third cases we modify the arterial and venous geometries to mimic two types of fistula that are created by surgery [48]. We then explicitly couple these modifications together within the coupling map.

Inlet flow to the arterial geometry in all cases was provided according to the profile in Figure 2(a). This was generated based on data presented in [15] for the right brachial artery. This profile was repeated in a cyclical manner.

3.1 Healthy vessels

To represent healthy vessels, we leave the entire geometry unmodified. The capillary bed consists of a single bed constructed by both arterial outlets and the 16 venous inlets in the hand region of the vascular structure.

In Figure 2 we present the total flow rate entering and exiting the forearm domain being modelled. For the parameters demonstrated here, it can be observed that a steady-state flow response is obtained within two heart-beat cycles.

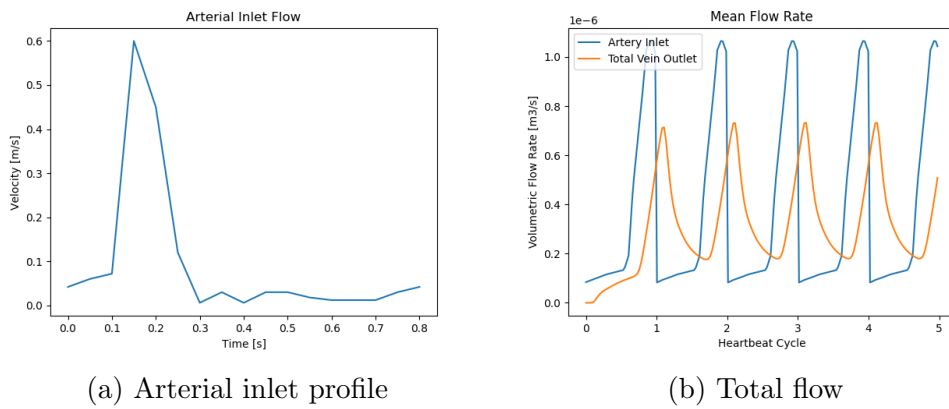


Figure 2: The left figure details a single cycle of the flow velocity provided to the inlet of the arterial geometry for all forearm flow cases. The right figure compares the total inlet and outlet flow rate through the healthy vessels.

3.2 Arteriovenous fistula - map model

Here we make use of the same vascular geometry as the healthy vessels but modify the coupling map to demonstrate how flow can be controlled with our scheme. In this case we construct separate beds for the two arterial outlets. Those venous inlets identified as feeding the cephalic vein were connected to the bed fed by the radial artery with the remainder fed by the ulnar artery.

The total entry and exit flow rate plots for this layout are presented in

Figure 3. Note here that the amplitude of the output flow rate in this configuration is reduced from what is seen in the healthy vessels. In Figure 3(b) we highlight the change in flow rate through the cephalic vein as a consequence of the modification to the mapping used. In this case, this can be seen to be an increase of approximately 40% and is coupled with a corresponding drop in flow through the basilic vein. This result also suggests that representing a modification to vascular geometry through the coupling map alone may not be the most effective approach.

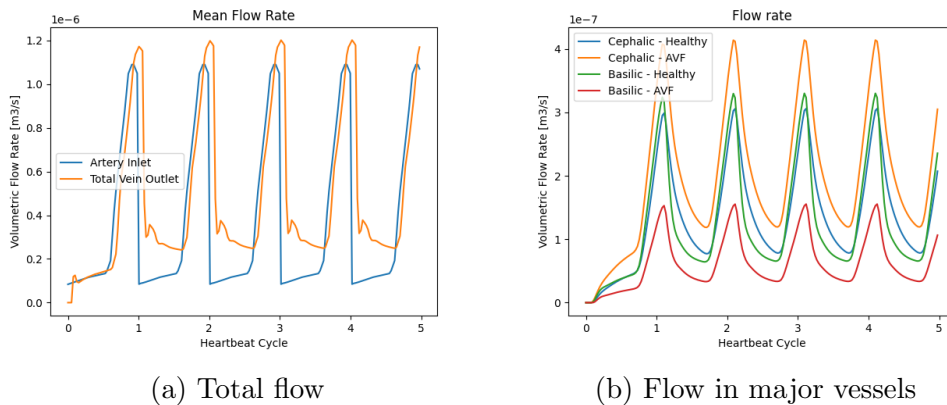


Figure 3: Flow rates through the forearm blood vessels with an arteriovenous fistula represented by a modification to the mapping scheme. The left figure indicates the total inlet and outlet flow of the system. The right figure compares flow exiting the major veins to that in the ‘healthy’ vessels.

In the following two sections we explicitly modify the vascular geometries to incorporate an arteriovenous fistula. We consider the end-to-side and side-to-side options of joining the cephalic vein to the radial artery. These are illustrated schematically in Figure 4.

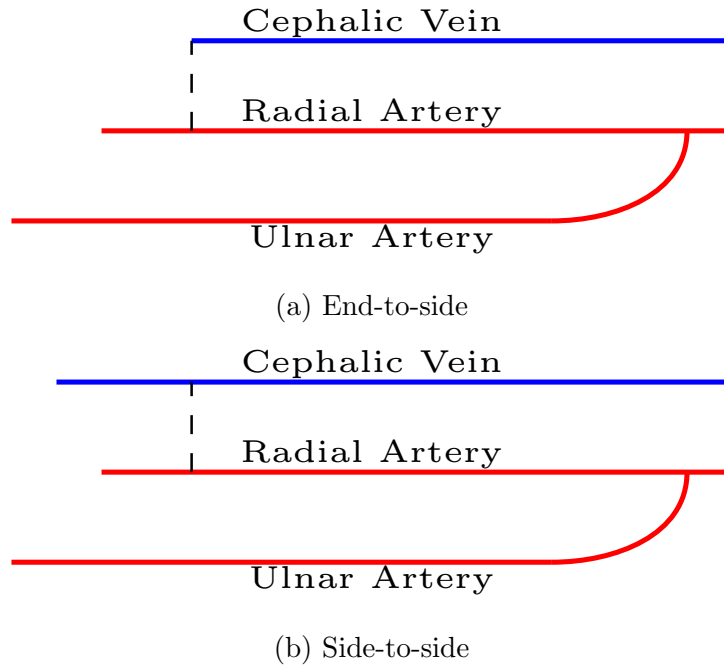


Figure 4: Schematic map of the geometry modification made to represent a end-to-side (upper) and side-to-side (lower) arteriovenous fistula. In the end-to-side case, the cephalic vein is terminated early and attached to the radial artery. The side-to-side case joins the two vessels through a hole made in their side.

3.3 End-to-side arteriovenous fistula - modified geometry 1

In this setting, we modify the venous geometry such that the cephalic vein is terminated ahead of a junction and mapped in a 1:1 fashion to an opening made in the radial artery.

In Figure 5, the change in flow pattern exiting the venous geometry can immediately be seen. The outlet flow rate now much more closely imitates the inlet flow profile provided to the arterial domain, particularly during the

initial impulse. The small jump in flow rate seen just after the main peak corresponds to return of flow passing through the capillary beds in the hand of the model. This can be noted through comparison to the outflow peaks in Figure 3. Figure 5(b) strongly demonstrates how this change in venous flow behaviour manifests in the major veins. The modification of the geometries has caused the peak flow exiting through the cephalic vein to increase by a factor of more than three. Flow exiting via the basilic vein has roughly halved as a consequence of this change but has maintained a similar profile shape due to it remaining to be fed by the flow through the capillary beds.

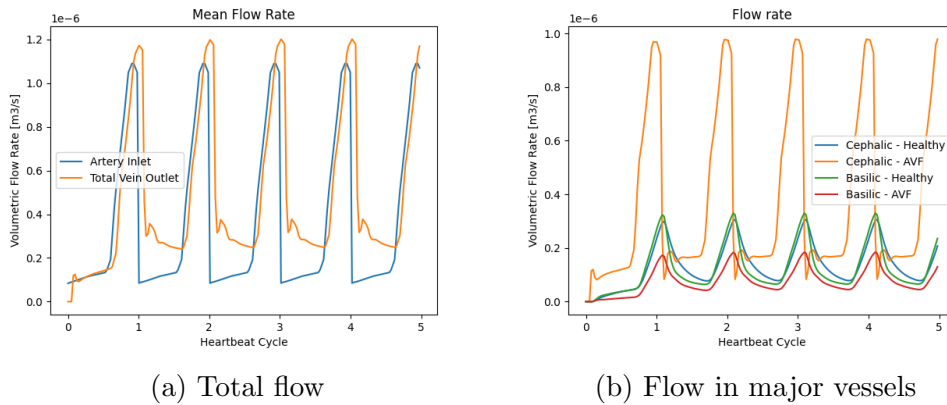


Figure 5: Flow rates through the forearm blood vessels with an arteriovenous fistula represented by the first geometric modification to the vessels. The left figure indicates the total inlet and outlet flow of the system. The right figure compares flow exiting the major veins to that in the ‘healthy’ vessels.

3.4 Side-to-side arteriovenous fistula - modified geometry 2

Here we represent an alternative construction of a fistula where the radial artery and cephalic vein are joined through the side of the vessels. Here flow from the artery can leak-off from the main flow through the vessel and supplement the returning flow through the vein. We again use a 1:1 coupling between these openings to allow flow to pass between them.

In Figure 6, it can be seen that the flow through the venous geometry becomes unstable, but not terminally so, after approximately 1 heartbeat. This is likely due to the inlet condition of the opening created in the cephalic vein being immediately adjacent to the main flow path. This replicates the formation of this fistula in practice. From a numerical perspective, the introduction of an entry tunnel to the created inlet should assist in improving the stability of the model. For the purposes of this discussion, we will focus on the stable section of flow which, in previous examples, has been repeated over the remaining heartbeats. In this portion of flow, the outlet flow rate has been significantly increased, even beyond that displayed in the first geometric modification. During the first heartbeat, Figure 6(b) indicates the flow through the cephalic vein increasing by a factor of approximately five. The flow through the basilic vein is reduced to around one-half of the original flow as a consequence of the increased flow through the cephalic vein.

The use of 3D flow simulations permits far more detailed visualisation of

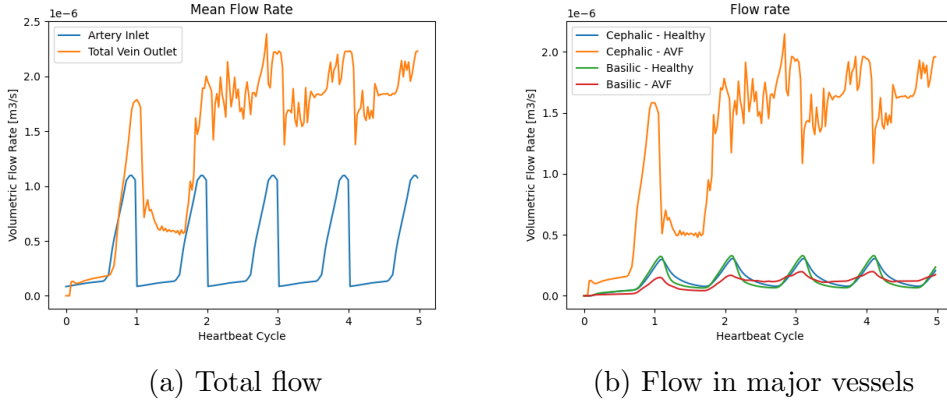


Figure 6: Flow rates through the forearm blood vessels with an arteriovenous fistula represented by the second geometric modification to the vessels. The left figure indicates the total inlet and outlet flow of the system. The right figure compares flow exiting the major veins to that in the ‘healthy’ vessels.

flow than is possible in 1D studies. This can be particularly informative for flow in patient-specific geometries. We provide an examples of flow through the arteries and veins of the healthy vessels and those with geometry modified arteriovenous fistula in Figure 7. The velocity field of the healthy vessels presented in Figure 7(a) here clearly captures the difference in flow through the radial artery (upper in figure) and the ulnar artery. In this case, it is due to the orientation of these vessels resulting from the bifurcation of the brachial artery. The distribution of flow to the venous inlets from the capillary bed can also be discerned in this figure. The interconnectedness of the veins leads to the reduction in flow velocity through the veins towards the exit plane at the right of the figure. In Figure 7(b) the change in flow pattern through the whole forearm vasculature as a consequence of creating the fistula can be clearly seen. Being able to observe such large-scale changes to flow is a key feature of our model being capable of simulating flow in large

vascular structures in 3D rather than just a smaller area of interest. The significant change in flow generated by the creation of the fistula can again be clearly observed in Figure 7(c). We infer that the increased turbulence in this style of junction generates the more chaotic flow pattern around the fistula connection sites.

4 Discussion

Within the healthy vessels, it can be noted that the specific flow rate in the cephalic vein (see Figure 3) is consistent with the lower end of the flow rates seen in the healthy control group in the study of arteriovenous fistula impacts on blood flow by Albayrak et al. [49]. This study collected 54 control patients and reported a flow rate in the cephalic vein of 28 ± 14 ml/min (mean \pm standard deviation). For the driving velocity used with our model we estimate an average flow velocity of 9 ml/min. This is consistent with the observations recorded in this clinical study. This result would also suggest that the overall input flow rate developed by our chosen profile (selected independently of the data in [49]) was less than what was observed in this study. The large standard deviation reported in observational fistula flow studies [49, 50] highlights how variable vascular flow can be between individuals.

In [50], a study of 71 patients who had an arteriovenous fistula created between the radial artery and cephalic vein is presented. Here the authors present a correlation between the diameter of the vein used to create the

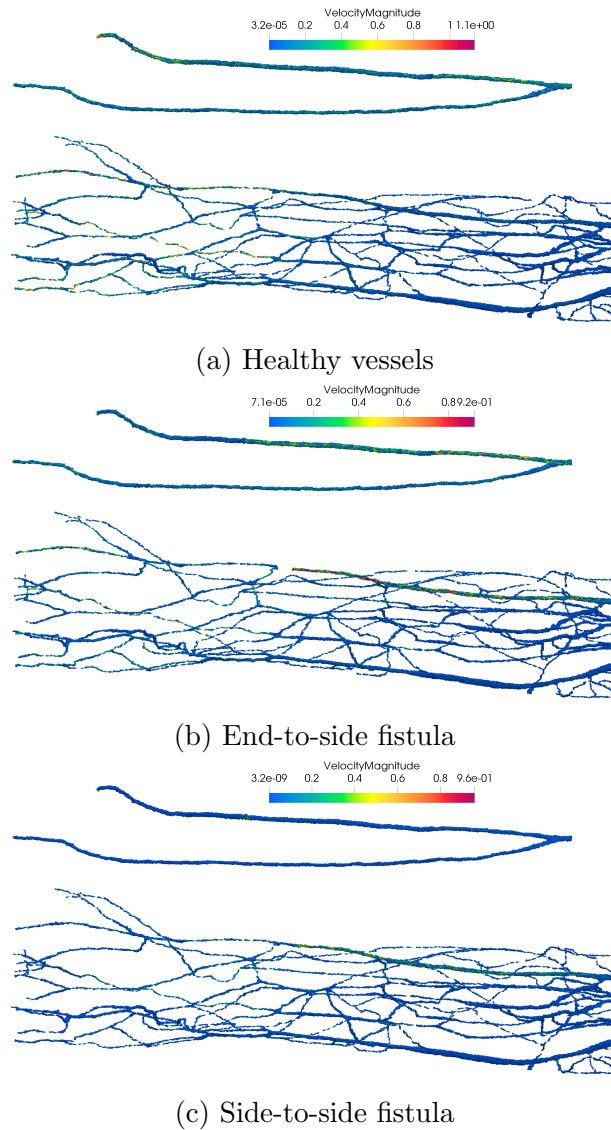


Figure 7: Flow fields through the arterial and venous domains, in all cases the arterial domain has been shifted upwards for clarity. This snapshot for the healthy and end-to-side fistula occurred after 1.4 s (700000 time steps) of simulation. That for the side-to-side fistula was captured after 0.8 s (400000 time steps).

fistula and the peroperative flow rate through it. In our model, the cephalic vein has a diameter of approximately 2.9 mm at the exit to the flow domain. For both of our modified geometries, around $1.0 \times 10^{-6} \text{ m}^3/\text{s}$ (60 ml/min) of

flow was generated through the cephalic vein. As indicated in Figure 8 this is consistent with the data presented in [50] and the correlation formed from it. We note here that we only study a single set of patient specific vessels. Using our model on a broader cross-section of vascular geometries would further inform the relationship between our model and the data gathered in [50].

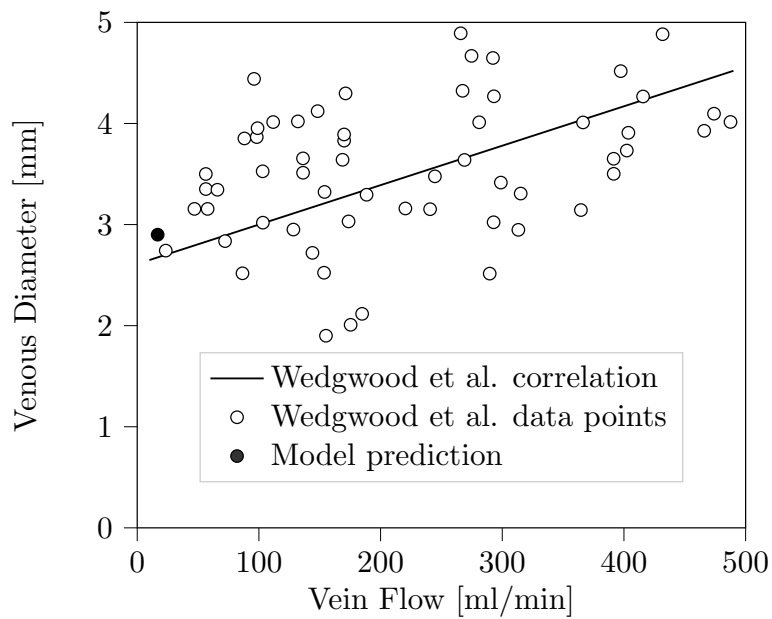


Figure 8: Comparison of cephalic vein flow rate calculated by our model and a correlation generated in Wedgwood et al. [50]. The data points of Wedgwood et al. with the range of the plot have also been indicated. The linear correlation of Wedgwood et al. has been extended here to encompass the presented data.

It is noted by Van Tricht et al. [48] that for the style of arteriovenous fistula studied in these examples a flow rate of at least 500 ml/min (8.33×10^{-6} m³/s) is required. This is around 20 times greater than the flow observed due to the physiological input to the cases presented here. It is also noted in [22] that the flow rate considered to be successful varies according to geographic

region. In all cases, the increase in flow to the cephalic vein will cause it to stretch and become stronger and larger allowing it to accommodate higher flow rates. As this maturation of a fistula may take weeks or months to complete, these effects cannot be captured immediately within our model. As a fundamentally conservative flow scheme, the LBM based approach we have used will only maintain the flow rate provided at the inlet. The rigid walls of our model do not permit the change in vascular geometry that occurs over the maturation time frame. However, these could be updated with new patient specific data in the case of follow-up monitoring. These considerations being noted, the significant increases in flow rate seen by all our fistula representations, but in particular the geometric modifications, illustrate how the considerable changes to flow distribution can be generated and studied within a numerical model.

The use of *in silico* models to pre-plan an operation means that surgeons can reduce the chance of performing an ineffectual procedure. In this paper we present a framework for studying 3D blood flow in human-scale vasculatures where the arteries and veins are coupled via a sub-scale capillary bed model. We demonstrate how two such models can accurately capture flow through a variety of configurations representative of human arterial-venous systems. Using these models we are able to capture peroperative flow rates through a surgically created arteriovenous fistula consistent with clinically observed data. This was observed for both an end-to-end and side-to-side style of fistula joining the radial artery and cephalic vein. The size and scale of the vascular networks used in our work is well beyond those used in exist-

ing 3D studies of fistula creation in the literature.

There are a number of features of our current model that can be improved in future work. In particular, we plan to accurately integrate the behaviour of elastic walls into our model to better represent how they change in response to flow. We will also continue our work in extending the coupling approaches outlined here to enable circulatory flow to be captured within a full-human systemic geometry of arteries and veins that is ultimately coupled to a 3D model of the heart. The framework of the virtual human permits such increases in fidelity or performance to be readily introduced.

The completion of these steps will constitute significant further progress along the pathway towards the virtual human. However, the culmination of this endeavour cannot be developed only from a simulation perspective. The ongoing development of close collaborations between modellers and clinicians will be critical in ensuring that its significant benefits for predictive medicine, patient outcomes and general wellbeing become accessible to all members of society.

Funding

We acknowledge funding support from European Commission CompBioMed Centre of Excellence (Grant No. 675451 and 823712). Support from the UK Engineering and Physical Sciences Research Council under the project ‘UK

Consortium on Mesoscale Engineering Sciences (UKCOMES)' (Grant No. EP/R029598/1) is gratefully acknowledged. We acknowledge funding support from MRC for a Medical Bioinformatics grant (MR/L016311/1), and special funding from the UCL Provost.

The authors gratefully acknowledge the Gauss Centre for Supercomputing e.V. (www.gauss-centre.eu) for funding this project by providing computing time on the GCS Supercomputer SuperMUC-NG at Leibniz Supercomputing Centre (www.lrz.de). This work used the ARCHER UK National Supercomputing Service (www.archer.ac.uk).

Acknowledgements

The authors acknowledge the Foundation for Research on Information Technologies in Society (IT²IS), particularly B. Lloyd and E. Neufeld, for providing the anatomical geometries used in this project as part of a collaboration within the CompBioMed Centre of Excellence.

References

- [1] P. Hunter, T. Chapman, P.V. Coveney, B. de Bono, V. Diaz, J. Fenner, A.F. Frangi, P. Harris, R. Hose, P. Kohl, P. Lawford, K. McCormack, M. Mendes, S. Omholt, A. Quarteroni, N.R. Shublaq, J. Skår, K. Stroetmann, J. Tegner, S.R. Thomas, I. Tollis, I. Tsamardinos, J.H.G.M. van

- Beek, and M. Viceconti. A vision and strategy for the virtual physiological human: 2012 update. *Interface Focus*, 3(2):20130004, 2013. doi: 10.1098/rsfs.2013.0004.
- [2] A. Muszkiewicz, O. J. Britton, P. Gemmell, E. Passini, C. Sánchez, X. Zhou, A. Carusi, T. A. Quinn, K. Burrage, A. Bueno-Orovio, and B. Rodriguez. Variability in cardiac electrophysiology: Using experimentally-calibrated populations of models to move beyond the single virtual physiological human paradigm. *Progress in Biophysics and Molecular Biology*, 120(1):115 – 127, 2016. doi: <https://doi.org/10.1016/j.pbiomolbio.2015.12.002>. Recent Developments in Biophysics & Molecular Biology of Heart Rhythm.
- [3] G. Biglino, C. Capelli, J. Bruse, G. M. Bosi, A. M. Taylor, and S. Schievano. Computational modelling for congenital heart disease: how far are we from clinical translation? *Heart*, 103(2):98–103, 2017. doi: 10.1136/heartjnl-2016-310423.
- [4] A. G. Hoekstra, E. van Bavel, M. Siebes, F. Gijzen, and L. Geris. Virtual physiological human 2016: translating the virtual physiological human to the clinic. *Interface Focus*, 8(1):20170067, 2018. doi: 10.1098/rsfs.2017.0067.
- [5] Y. Kim, O. Hatley, S. Rhee, S. Yi, H. A. Lee, S. Yoon, J. Chung, K. Yu, and H. Lee. Development of a korean-specific virtual population for physiologically based pharmacokinetic modelling and simula-

- tion. *Biopharmaceutics & Drug Disposition*, 40(3-4):135–150, 2019. doi: 10.1002/bdd.2178.
- [6] S. E. Morton, J. L. Knopp, J. G. Chase, K. Müller, P. Docherty, G. M. Shaw, and M. Tawhai. Predictive virtual patient modelling of mechanical ventilation: Impact of recruitment function. *Annals of Biomedical Engineering*, 47(7):1626–1641, 2019. doi: <https://doi.org/10.1007/s10439-019-02253-w>.
- [7] T. W. Hokken, J. M. Ribeiro, P. P. De Jaegere, and N. M. Van Mieghem. Precision medicine in interventional cardiology. *Interventional Cardiac Review*, 15(3), 2020. doi: <https://doi.org/10.15420/icr.2019.23>.
- [8] P. Hunter, P.V. Coveney, B. de Bono, V. Diaz, J. Fenner, A.F. Frangi, P. Harris, R. Hose, P. Kohl, P. Lawford, K. McCormack, M. Mendes, S. Omholt, A. Quarteroni, J. Skår, J. Tegner, S.R. Thomas, I. Tollis, I. Tsamardinos, J.H.G.M. van Beek, and M. Viceconti. A vision and strategy for the virtual physiological human in 2010 and beyond. *Philosophical Transactions of the Royal Society A: Mathematical, Physical and Engineering Sciences*, 368(1920):2595–2614, 2010. doi: 10.1098/rsta.2010.0048.
- [9] D. Noble. A theory of biological relativity: no privileged level of causation. *Interface Focus*, 2(1):55–64, 2012. doi: 10.1098/rsfs.2011.0067.
- [10] N. Xiao, J. D. Humphrey, and C. A. Figueroa. Multi-scale computational model of three-dimensional hemodynamics within a deformable full-body arterial network. *Journal of Computational Physics*, 244:22

- 40, 2013. doi: <https://doi.org/10.1016/j.jcp.2012.09.016>. Multi-scale Modeling and Simulation of Biological Systems.
- [11] A. Randles, E. W. Draeger, and P.E. Bailey. Massively parallel simulations of hemodynamics in the primary large arteries of the human vasculature. *Journal of Computational Science*, 9:70 – 75, 2015. doi: <https://doi.org/10.1016/j.jocs.2015.04.003>. Computational Science at the Gates of Nature.
- [12] C. Sheng, S.N. Sarwal, K.C. Watts, and A.E. Marble. Computational simulation of blood flow in human systemic circulation incorporating an external force field. *Medical and Biological Engineering and Computing*, 33(1):8–17, Jan 1995. doi: 10.1007/BF02522938.
- [13] M.U. Qureshi, G.D.A. Vaughan, C. Sainsbury, M. Johnson, C.S. Peskin, M.S. Olufsen, and N.A. Hill. Numerical simulation of blood flow and pressure drop in the pulmonary arterial and venous circulation. *Biomechanics and Modeling in Mechanobiology*, 13(5):1137–1154, Oct 2014. doi: 10.1007/s10237-014-0563-y.
- [14] L. O. Müller and E. F. Toro. A global multiscale mathematical model for the human circulation with emphasis on the venous system. *International Journal for Numerical Methods in Biomedical Engineering*, 30(7):681–725, 2014. doi: 10.1002/cnm.2622.
- [15] J. P. Mynard and J. J. Smolich. One-dimensional haemodynamic modeling and wave dynamics in the entire adult circulation. *Annals of Biomedical Engineering*, 43(6):1443–1460, 2015.

- [16] J. W. S. McCullough, R. A. Richardson, A. Patronis, R. Halver, R. Marshall, M. Ruefenacht, B. J. M. Wylie, T. Odaker, M. Wiedemann, B. Lloyd, E. Neufeld, G. Sutmann, A. Skjellum, D. Kranzlmüller, and P. V. Coveney. Towards blood flow in the virtual human: Efficient self-coupling of HemeLB. *J R Soc Interface Focus*, in press 2020. doi: <https://doi.org/10.1098/rsfs.2019.0119>.
- [17] D. Groen, J. Hetherington, H.B. Carver, R.W. Nash, M.O. Bernabeu, and P.V. Coveney. Analysing and modelling the performance of the HemeLB lattice-Boltzmann simulation environment. *Journal of Computational Science*, 4(5):412 – 422, 2013. doi: <https://doi.org/10.1016/j.jocs.2013.03.002>.
- [18] D. Groen, R.A. Richardson, R. Coy, U.D. Schiller, H. Chandrashekar, F. Robertson, and P.V. Coveney. Validation of patient-specific cerebral blood flow simulation using transcranial doppler measurements. *Frontiers in Physiology*, 9:721, 2018. doi: [10.3389/fphys.2018.00721](https://doi.org/10.3389/fphys.2018.00721).
- [19] J. Latt, O. Malaspinas, D. Kontaxakis, A. Parmigiani, D. Lagrava, F. Brogi, M. Ben Belgacem, Y. Thorimbert, S. Leclaire, S. Li, F. Marson, J. Lemus, C. Kotsalos, R. Conradin, C. Coreixas, R. Petkantchin, F. Raynaud, J. Beny, and B. Chopard. Palabos: Parallel lattice Boltzmann solver. *Computers & Mathematics with Applications*, 2020. doi: <https://doi.org/10.1016/j.camwa.2020.03.022>.
- [20] J.O.S.H. Cleary and A.R. Guimaraes. Magnetic Resonance Imaging. In Linda M. McManus and Richard N. Mitchell, editors, *Patho-*

- biology of Human Disease*, pages 3987 – 4004. Academic Press, San Diego, 2014. ISBN 978-0-12-386457-4. doi: <https://doi.org/10.1016/B978-0-12-386456-7.07609-7>. URL <http://www.sciencedirect.com/science/article/pii/B9780123864567076097>.
- [21] Eugene Lin and Adam Alessio. What are the basic concepts of temporal, contrast, and spatial resolution in cardiac CT? *Journal of Cardiovascular Computed Tomography*, 3(6):403–408, August 2009. doi: 10.1016/j.jcct.2009.07.003.
- [22] M. Allon and M. L. Robbin. Increasing arteriovenous fistulas in hemodialysis patients: Problems and solutions. *Kidney International*, 62(4):1109 – 1124, 2002. doi: <https://doi.org/10.1111/j.1523-1755.2002.kid551.x>.
- [23] K. Tullett. Renal vascular access - having a fistula for haemodialysis. Online, December 2019. URL <https://www.uhb.nhs.uk/Downloads/pdf/PiRenalVascularAccess.pdf>.
- [24] A. S. Bode, W. Huberts, E. M. H. Bosboom, W. Kroon, W. P. M. van der Linden, R. N. Planken, F. N. van de Vosse, and J. H. M. Tordoir. Patient-specific computational modeling of upper extremity arteriovenous fistula creation: Its feasibility to support clinical decision-making. *PLOS ONE*, 7(4):1–8, 04 2012. doi: 10.1371/journal.pone.0034491.
- [25] I. Decorato, Z. Kharboutly, T. Vassallo, J. Penrose, C. Legallais, and A. Salsac. Numerical simulation of the fluid structure interactions in a compliant patient-specific arteriovenous fistula. *International Journal*

- for *Numerical Methods in Biomedical Engineering*, 30(2):143–159, 2014.
doi: 10.1002/cnm.2595.
- [26] S. Manini, K. Passera, W. Huberts, L. Botti, L. Antiga, and A. Remuzzi. Computational model for simulation of vascular adaptation following vascular access surgery in haemodialysis patients. *Computer Methods in Biomechanics and Biomedical Engineering*, 17(12):1358–1367, 2014. doi: 10.1080/10255842.2012.745857. PMID: 23281788.
- [27] P. M. McGah, D. F. Leotta, K. W. Beach, and A. Aliseda. Effects of wall distensibility in hemodynamic simulations of an arteriovenous fistula. *Biomechanics and Modeling in Mechanobiology*, 13(3):679–695, 2014.
- [28] N. Zonnebeld, W. Huberts, M. M. van Loon, T. Delhaas, and J. H.M. Tordoir. Preoperative computer simulation for planning of vascular access surgery in hemodialysis patients. *The Journal of Vascular Access*, 18(1_suppl):S118–S124, 2017. doi: 10.5301/jva.5000661. PMID: 28297050.
- [29] Z. Bai and L. Zhu. Simulation of blood flow past a distal arteriovenous-graft anastomosis at low Reynolds numbers. *Physics of Fluids*, 31(9):091902, 2019. doi: 10.1063/1.5099635.
- [30] HemeLB, 2019. URL www.hemelb.org.
- [31] S. Succi. *The Lattice Boltzmann Equation for Fluid Dynamics and Beyond*. Oxford University Press, Oxford, 2001.

- [32] A.A. Mohamad. *Lattice Boltzmann Method: Fundamentals and Engineering Applications with Computer Codes*. Springer London, 2011.
- [33] Z. Guo and C. Shu. *Lattice Boltzmann Method and Its Applications in Engineering*. WORLD SCIENTIFIC, 2013. doi: 10.1142/8806. URL <https://www.worldscientific.com/doi/abs/10.1142/8806>.
- [34] T. Krüger, H. Kusumaatmaja, A. Kuzmin, O. Shardt, G. Silva, and E.M. Viggen. *The Lattice Boltzmann Method: Principles and Practice*. Springer, 2017. doi: 10.1007/978-3-319-44649-3.
- [35] S. Succi. *The Lattice Boltzmann Equation: For Complex States of Flowing Matter*. Oxford University Press, Oxford, 2018. URL <https://www.oxfordscholarship.com/10.1093/oso/9780199592357.001.0001/oso-9780199592357>.
- [36] M.D. Mazzeo and P.V. Coveney. HemeLB: A high performance parallel lattice-Boltzmann code for large scale fluid flow in complex geometries. *Computer Physics Communications*, 178(12):894 – 914, 2008. doi: <https://doi.org/10.1016/j.cpc.2008.02.013>.
- [37] M.O. Bernabeu, M.L. Jones, J.H. Nielsen, T. Krüger, R.W. Nash, D. Groen, S. Schmieschek, J. Hetherington, H. Gerhardt, C.A. Franco, and P.V. Coveney. Computer simulations reveal complex distribution of haemodynamic forces in a mouse retina model of angiogenesis. *Journal of The Royal Society Interface*, 11(99):20140543, 2014. doi: 10.1098/rsif.2014.0543.

- [38] M. O. Bernabeu, R. W. Nash, D. Groen, H. B. Carver, J. Hetherington, T. Krüger, and P. V. Coveney. Impact of blood rheology on wall shear stress in a model of the middle cerebral artery. *Interface Focus*, 3(2): 20120094, 2013. doi: 10.1098/rsfs.2012.0094.
- [39] C. A. Franco, M. L. Jones, M. O. Bernabeu, I. Geudens, T. Mathivet, A. Rosa, F. M. Lopes, A. P. Lima, A. Ragab, R. T. Collins, L. Phng, P. V. Coveney, and H. Gerhardt. Dynamic Endothelial Cell Rearrangements Drive Developmental Vessel Regression. *PLOS Biology*, 13(4): 1–19, 04 2015. doi: 10.1371/journal.pbio.1002125.
- [40] C. A. Franco, M. L. Jones, M. O. Bernabeu, A. Vion, P. Barbacena, J. Fan, T. Mathivet, C. G. Fonseca, A. Ragab, T. P. Yamaguchi, P. V. Coveney, R. A. Lang, and H. Gerhardt. Non-canonical Wnt signalling modulates the endothelial shear stress flow sensor in vascular remodelling. *eLife*, 5:e07727, feb 2016. doi: 10.7554/eLife.07727.
- [41] A. Patronis, R.A. Richardson, S. Schmieschek, B.J.N. Wylie, R.W. Nash, and P.V. Coveney. Modeling patient-specific magnetic drug targeting within the intracranial vasculature. *Frontiers in Physiology*, 9: 331, 2018. doi: 10.3389/fphys.2018.00331.
- [42] R.W. Nash, H.B. Carver, M.O. Bernabeu, J. Hetherington, D.K. Groen, T. Krüger, and P.V. Coveney. Choice of boundary condition for lattice-Boltzmann simulation of moderate-Reynolds-number flow in complex domains. *Phys. Rev. E*, 89:023303, Feb 2014. doi: 10.1103/PhysRevE.89.023303.

- [43] M. Bouzidi, M. Firdaouss, and P. Lallemand. Momentum transfer of a Boltzmann-lattice fluid with boundaries. *Physics of Fluids*, 13(11): 3452–3459, 2001. doi: 10.1063/1.1399290.
- [44] Z. Guo, C. Zheng, and B. Shi. Discrete lattice effects on the forcing term in the lattice Boltzmann method. *Phys. Rev. E*, 65:046308, Apr 2002. doi: 10.1103/PhysRevE.65.046308.
- [45] Human Models - Yoon-sun, 2019. URL <https://itis.swiss/virtual-population/virtual-population/vip3/yoon-sun/>.
- [46] A. Christ, W. Kainz, E.G. Hahn, K. Honegger, M. Zefferer, E. Neufeld, W. Rascher, R. Janka, W. Bautz, J. Chen, B. Kiefer, P. Schmitt, H.-P. Hollenbach, J. Shen, M. Oberle, D. Szczerba, A. Kam, J.W. Guag, and N. Kuster. The Virtual Family - development of surface-based anatomical models of two adults and two children for dosimetric simulations. *Physics in Medicine and Biology*, 55(2):N23, 2010. doi: 10.1088/0031-9155/55/2/N01.
- [47] M. Gosselin, E. Neufeld, H. Moser, E. Huber, S. Farcito, L. Gerber, M. Jedensjö, I. Hilber, F. Di Gennaro, B. Lloyd, et al. Development of a new generation of high-resolution anatomical models for medical device evaluation: the Virtual Population 3.0. *Physics in Medicine & Biology*, 59(18):5287, 2014. doi: 10.1088/0031-9155/59/18/5287.
- [48] I. Van Tricht, D. De Wachter, J. Tordoir, and P. Verdonck. Hemodynamics and complications encountered with arteriovenous fistulas and grafts

- as vascular access for hemodialysis: A review. *Annals of Biomedical Engineering*, 33(9):1142–1157, 2005.
- [49] R. Albayrak, S. Yuksel, M. Colbay, B. Degirmenci, G. Acarturk, A. Haktanir, and O. Karaman. Hemodynamic changes in the cephalic vein of patients with hemodialysis arteriovenous fistula. *Journal of Clinical Ultrasound*, 35(3):133–137, 2007. doi: 10.1002/jcu.20307.
- [50] K. R. Wedgwood, P. A. Wiggins, and P. J. Guillou. A prospective study of end-to-side vs. side-to-side arteriovenous fistulas for haemodialysis. *British Journal of Surgery*, 71(8):640–642, 1984. doi: 10.1002/bjs.1800710831.
- [51] J. P. Mynard and K. Valen-Sendstad. A unified method for estimating pressure losses at vascular junctions. *International Journal for Numerical Methods in Biomedical Engineering*, 31(7), 2015. doi: 10.1002/cnm.2717.

5 Supplementary Information

Alternative sub-scale method for capillary beds

5.1 Method outline

The second model for capillary beds is based on resistor-capacitor models used in some existing models as capillary beds or windkessel boundary conditions. We have taken particular inspiration from the works of Mynard et al. [15, 51]. In our approach we firstly determine the flow weighted velocity, v_D on the arterial and venous sides of a capillary bed

$$v_D = \sum_j \frac{A_j v_j^2}{A_j v_j}. \quad (3)$$

The flow rate, Q , can then be determined by scaling v_D by the total area of the appropriate vessels. We then consider the capillary bed as the conceptual model presented in Figure 9. Here the bed has capacitance, \bar{C} , and resistance, R . The change in pressure over the bed is computed as $\Delta P = RQ_B$ where Q_B is the flow through the bed itself. Taking capacitance into account, the flow of the system can be described as

$$Q_A - \bar{C} \frac{d\bar{P}}{dt} = Q_V, \quad (4)$$

where $\bar{P} = 0.5(P_A + P_V)$ is the average pressure of the system. We note that this can be recast as $\bar{P} = P_A - 0.5(P_A - P_V) = P_A - 0.5RQ_B$. We assume that the majority of the pressure change arises on the venous side of

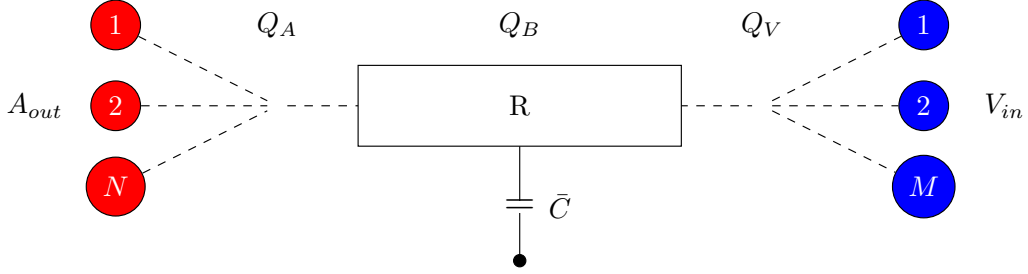


Figure 9: Conceptual layout of the resistor-capacitor based approach to representing the capillary beds. The arterial, Q_A and venous, Q_V flow through the bed is accumulated from and distributed to the connecting vessels by their relative portion of the total vessel area attached to the bed. The capacitance, \bar{C} , can be viewed as an average of arterial and venous vessel capacitances.

the system, leading to

$$\frac{d\bar{P}}{dt} \approx \frac{d}{dt} - 0.5RQ_B = -0.5R\frac{dQ_B}{dt}. \quad (5)$$

This then results in

$$Q_A + 0.5\bar{C}R\frac{dQ_B}{dt} = Q_V, \quad (6)$$

which can be used to update the flow rate on the receiving side of the capillary coupling. This is then distributed to the individual vessels based on the relative area of each.

Results

All test cases presented in the main text were also conducted with this alternative approach. For this method, we set $\bar{C}R = 0.013125$, a value adapted based on those used in [15]. The performance of this model was comparable both in terms of output and simulation time to those reported in the main text. Here we present the main results for this method.

5.2 Healthy vessels

Figure 10 we present the corresponding results to Figure 2 of the main text.

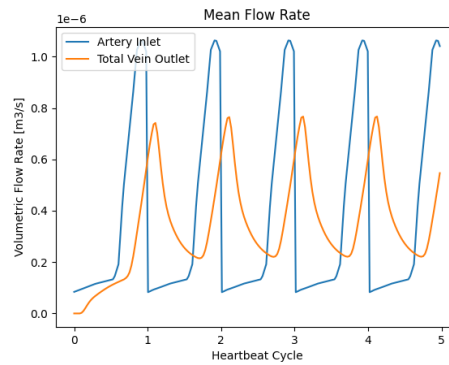


Figure 10: Comparison of the total inlet and outlet flow rate through the healthy vessels for the alternative sub-scale methods.

5.3 Arteriovenous fistula - map model

Figure 11 we present the corresponding results to Figure 3 of the main text.

Here, this change in flow through the cephalic vein is much less dramatic than in the main text - only around 7% - although a notable drop in flow through the basilic vein is present. This illustrates the difference in how the two sub-scale models distribute flow within a bed.

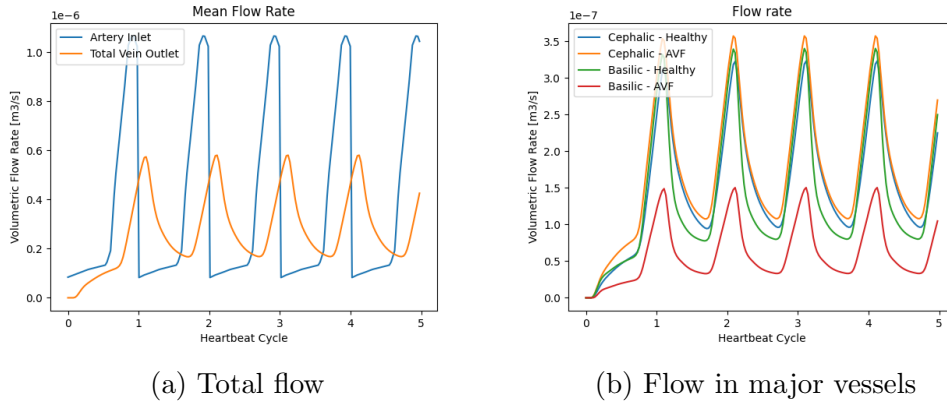


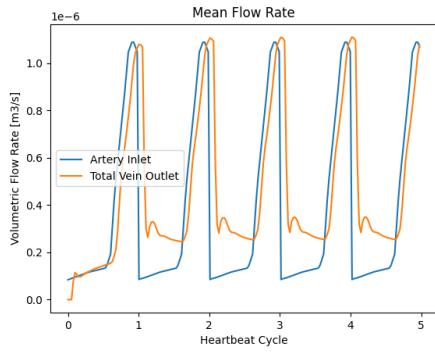
Figure 11: Flow rates through the forearm blood vessels with an arteriovenous fistula represented by a modification to the mapping scheme. The upper figures indicate the total inlet and outlet flow of the system. The lower figures compare flow exiting the major veins to that in the ‘healthy’ vessels.

5.4 End-to-side arteriovenous fistula - modified geometry 1

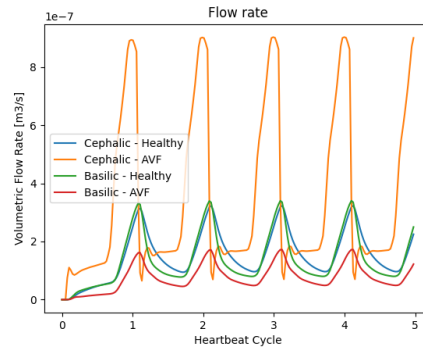
Figure 12 we present the corresponding results to Figure 5 of the main text.

5.5 Side-to-side arteriovenous fistula - modified geometry 2

Figure 13 we present the corresponding results to Figure 6 of the main text.

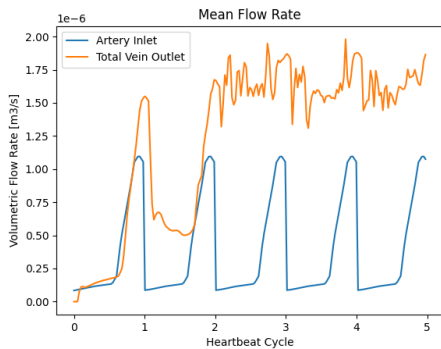


(a) Total flow

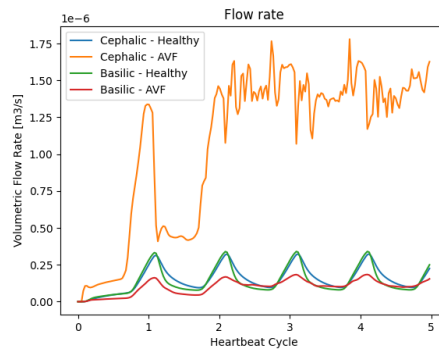


(b) Flow in major vessels

Figure 12: Flow rates through the forearm blood vessels with an arteriovenous fistula represented by the first geometric modification to the vessels. The upper figure indicate the total inlet and outlet flow of the system. The lower figure compare flow exiting the major veins to that in the ‘healthy’ vessels.



(a) Total flow



(b) Flow in major vessels

Figure 13: Flow rates through the forearm blood vessels with an arteriovenous fistula represented by the second geometric modification to the vessels. The upper figures indicate the total inlet and outlet flow of the system. The lower figures compare flow exiting the major veins to that in the ‘healthy’ vessels.